

High numerical aperture in multimode microstructured optical fibers

Nader A. Issa

Microstructured or “air-clad” fibers, with air holes surrounding a large core, have recently demonstrated much wider light-acceptance angles than conventional fibers. An original and accurate method is presented for determining the numerical aperture of such fibers using leaky modes. The dependence on length, wavelength, and various microstructure dimensions are evaluated for the first time for a class of fibers that exhibit exceptionally high numerical apertures. These results show excellent agreement with published measurements on similar fibers and verify that bridge thicknesses much smaller than the wavelength are required for high numerical apertures. © 2004 Optical Society of America
OCIS codes: 060.2280, 230.3990.

1. Introduction

Multimode optical fibers with wide light-acceptance angles and high trapping efficiency are essential for a variety of applications. In recent years, they have become increasingly important in such fields as the detection of charged particles and ionizing radiation,¹ multiobject spectroscopy,² and, most notably, for cladding pumped fiber lasers.³ Their application in short-distance communication has a long history owing to their ease of connectivity and high launching efficiency. More recently, however, their usefulness in the interconnection of electronic systems over very short distances is being recognized.⁴

In order to quantify the capture of light from large-area, broad-beam sources, or the trapping of light emissions from within the fiber core, the nominal numerical aperture (NA) is generally defined for optical fibers as

$$NA = \sin(\theta_{\max}), \quad (1)$$

where θ_{\max} is the maximum angle at which a *meridional* ray entering the fiber will be guided. It is

measured from the half-angle at which the far-field angular intensity distribution has decreased to a standard 5% of its maximum value. High NA values ranging from 0.37 in doped silica fiber to 0.66 in teflon-coated fibers⁵ are not uncommon. Yet these values can be considerably lower than the NAs achievable in multimode microstructured optical fibers, for which values ranging from 0.4 to higher than 0.9 have recently been reported.^{3,6–10} The concept of air-clad optical fibers for realizing an exceptionally high NA is an old one,¹¹ and many subsequent design variations have concentrated on methods to address the obvious practical difficulties of supporting the core in its air cladding. While the mechanical properties of thick supporting bridges are highly desirable, these bridges provide core light with an avenue for leakage, and little is currently known about the dependence of optical performance on bridge thickness and geometry or on fiber length. A typical class of air-clad fiber, shown in Fig. 1(c), is studied here. The NA is determined from an analysis of leaky modes supported by the fiber, providing accurate solutions with a simple physical interpretation.

Conventional multimode fibers have been modeled accurately by the ray method.^{1,5,12} This method however, is incapable of correctly describing the scattering of light off subwavelength features nor optical tunneling through short evanescent regions (frustrated total internal reflection). A local-plane-wave approach can supplement this method by solving for the reflection matrices of the “flattened” microstructured array. The overall fiber transmission is dictated then by the total number of reflections along the fiber length. While this approach has the merit of

Nader Issa (n.issa@ofc.usyd.edu.au) is with the Optical Fibre Technology Centre, Australian Photonics Cooperative Centre, University of Sydney, 206 National Innovation Centre, Australian Technology Park, Eveleigh, New South Wales 1430, Australia, and the School of Physics, University of Sydney, New South Wales 2006, Australia.

Received 3 April 2004; revised manuscript received 7 August 2004; accepted 13 August 2004.

0003-6935/04/336191-07\$15.00/0

© 2004 Optical Society of America

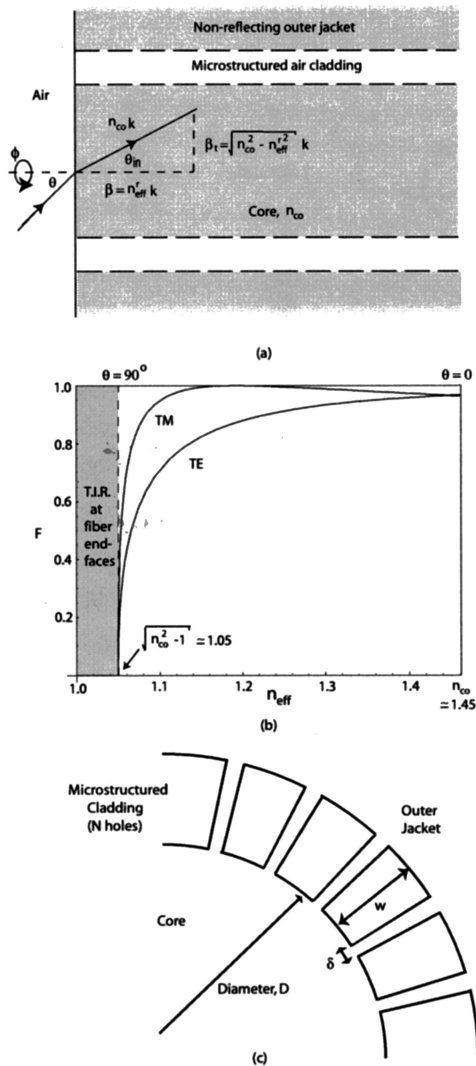


Fig. 1. (a) Cross section along optical fiber axis. The core refractive index, $n_{co} = 1.45$, is assumed equal to the index of the infinite jacket. Both are lossless. (b) Fresnel reflection at fiber end faces for TE and TM polarized light. Total internal reflection (TIR) occurs at the fiber end faces when $n_{eff} \leq (n_{co}^2 - 1)^{1/2}$ or $\theta_{in} \geq \arcsin(1/n_{co})$. (c) Schematic of air-clad fiber geometry studied here.

simple conceptual understanding, it is no less computationally demanding than the leaky-mode approach proposed here. In fact, excellent agreement between these two approaches is shown here for the simplified problem of a continuous air ring of finite radial width w . A disadvantage of the local-plane-wave method is highlighted here by the small disagreement when $w/\lambda \ll 1$, where the number of guided modes in a given length becomes small. In this extreme, the modal nature of the waveguide is not represented by plane-wave approximations.

Another method models the radiation of power into free space from the end face of the fiber. This has been successfully applied to the NA of single-mode microstructured fibers,¹³ but for multimode fibers, knowledge of the final distribution of power between

the guided modes is of greatest importance. Beam propagation can be used to quantify confinement losses during propagation; however, given the large dynamic range of confinement losses, such computations are usually prohibitive.

An alternative, but heuristic, estimate of NA can be obtained by a form of local mode coupling. It assumes that core modes efficiently couple to fictitious but transient modes localized in the microstructured bridges (or cladding) when their effective indices match. Once these bridge modes are excited, they quickly propagate power into the outer jacket. The fundamental bridge mode, with effective index n_b , then provides the cutoff condition for guidance in the core, rather than the cladding index in conventional fibers. The NA is subsequently defined by $\overline{NA} = (n_{co}^2 - n_b^2)^{1/2}$. This highly simplified technique has been shown to provide an excellent estimate of the experimentally measured NA in fibers by Bouwmans *et al.*⁷ and very recently by Wadsworth *et al.*⁸ Furthermore, it is shown here to be consistent with present full calculations. Wadsworth *et al.* make a comparison of this simplified model with the numerical aperture as determined solely by the fictitious cladding mode in the “flattened” microstructured cladding. While these simplifications are highly convenient for many structures, they remain heuristic and are limited to fibers that have either an obvious choice for a localized bridge mode or a relatively wide cladding. In addition, they provide no information on the dependence of NA on fiber or bridge length.

2. Outline of Method

Unlike the truly bound modes of conventional fibers, the majority of propagated power in microstructured and air-clad fibers is often via leaky modes. Physically, light is confined by the enclosure of airholes, and loss arises from power leakage between and through the holes. Leaky modes provide a highly effective description of the propagation process in such waveguides.¹⁴ They are eigensolutions of the vector-wave equation and are characterized by a complex longitudinal component of the wave vector, $\beta = kn_{eff}$, where $k = 2\pi/\lambda$ and $n_{eff} = n_{eff}^r + in_{eff}^i$ is the complex mode effective index. Power attenuation from confinement loss is given simply by $\exp(-2n_{eff}^i kL)$, where L is the length of the fiber. Leaky modes are chosen as the analytic tool for this paper because they arise naturally from the simplest boundary conditions that can be imposed on the waveguide problem, that no light radiated from the microstructured region is reflected back. In this paper, the excitation of groups of leaky modes is addressed with a simplified physical approach; however, in order to calculate the precise excitation of individual leaky-mode fields, a more sophisticated mathematical process is required.¹⁵ A highly absorbing outer jacket, similar to the coatings used in real optical fibers, may be used in numerical calculations. This may serve the purpose of avoiding the

use of leaky modes, potentially at the cost of greatly increasing the computation domain and therefore computational resources. Furthermore, the choice of jacket position and constitution would then require justification and introduce spurious modes into the calculation. It is assumed here that the backreflection from such a jacket is negligible, so that losses are closely approximated by confinement loss, as predicted by the leaky-mode solutions.

Within the core, the wave vector of a mode is decomposed into its longitudinal and transverse components [see Fig. 1(a)]. Thus an effective index uniquely specifies an internal angle, θ_{in} , and the external angle,

$$\theta = \sin^{-1}(\sqrt{n_{co}^2 - n_{eff}^r{}^2}), \quad (2)$$

can be derived using Snell's law. Similarly, the neighborhood of any external angle, $\theta \pm \Delta\theta/2$, maps to an interval of effective index, $n_{eff}^r(\theta) \pm \Delta n_{eff}^r(\theta)/2$, within which a typical fiber will support only a finite number of leaky modes, M .

Now consider a source of area A that is much smaller than the fiber core. When placed close to the fiber end face and centered within the core, such a source is expected to launch only near-meridional rays. The power radiated by the source within a narrow angular range $\theta \pm \Delta\theta/2$ is given by^{12,16}

$$P(\theta) = A \int_0^{2\pi} \int_{\theta-\Delta\theta/2}^{\theta+\Delta\theta/2} I(\theta') \sin(\theta') d\theta' d\phi \\ \simeq 2\pi A I(\theta) \sin(\theta) \Delta\theta, \quad (3)$$

for both TE and TM polarizations and where $I(\theta)$ is the angular intensity distribution. For a diffuse source that obeys Lambert's (cosine) law, $I(\theta) = I_o \cos(\theta)$. Apart from Fresnel reflections at the end faces, the only remaining source of loss is confinement loss. For this, it is assumed that this power is transmitted equally and only via the leaky modes with n_{eff}^r in the range $n_{eff}^r(\theta) \pm \Delta n_{eff}^r(\theta)/2$ determined from Eq. (2). Thus for a normalized source the *far-field* angular transmission, or intensity distribution (power per unit solid angle), upon exiting the fiber becomes

$$T(\theta) \simeq \frac{P(\theta) \left[\frac{F_{TE}(\theta) + F_{TM}(\theta)}{2} \right]^2 \alpha(\theta)}{2\pi A \sin(\theta) \Delta\theta} \\ = I(\theta) \left[\frac{F_{TE}(\theta) + F_{TM}(\theta)}{2} \right]^2 \alpha(\theta), \quad (4)$$

where

$$\alpha(\theta) = \frac{1}{M} \sum_{m=1}^M \exp(-2\{n_{eff}^i\}_m kL), \quad (5)$$

is the averaged transmission via leaky modes in the range $n_{eff}^r(\theta) \pm \Delta n_{eff}^r(\theta)/2$. The terms F_{TE} and F_{TM} account for the angular and polarization dependence of Fresnel reflective losses entering *and* leaving the

fiber. Its importance at large angles is obvious from Fig. 1(b), as it prevents a theoretical NA > 1. In fact, it is possible for an air-clad silica fiber ($n_{co} \simeq 1.45$) to support modes with $n_{eff}^r < (n_{co}^2 - 1)^{1/2} \simeq 1.05$ when the measured NA is close to 1. These modes experience total internal reflection even at the end faces of the fiber and therefore cannot be excited by external launching. When an application requires the efficient detection of light generated from within the fiber core, it may be important to provide index matching between the fiber end face and detector to extract the light in these modes.

The simple interpretation of Eq. (4) is that far-field transmission for an incident angle is evaluated by averaging the transmission via modes that are excited in a narrow range about that angle. Such averaging is necessary, since confinement losses are strongly dependent on the polarization of the mode (or mode class) at large θ_{in} . Recall that the definition of NA is for meridional rays only. In a modal picture, this implies that the only relevant mode class to consider is the TE_{0n} -like and TM_{0n} -like modes, which are strictly only TE or TM for cylindrically symmetric fibers. However, HE_{mn} -like and EH_{mn} -like mode classes have also been included in the analysis of Section 6, since they play a dominant role in power propagation in real fiber systems, as well as have the property of nearly zero skewness when m is a small integer. That is, $|\beta_\phi|^2 \ll (n_{co}k)^2$, where the transverse component of the wave vector is decomposed in polar coordinates $\beta_t^2 = \beta_r^2 + \beta_\phi^2$.¹⁷ Depending on the numerical method used for the calculation of leaky modes, these mode classes can be selected in different but straightforward ways. On the other hand, modes with large skewness behave quite differently. Fortunately, these modes are generally difficult to launch, partially because of their distance from the fiber center as well as the higher Fresnel reflection they experience at end faces. The current definition therefore remains useful for practical purposes,^{1,5,18} but it is important to note that the inclusion of skew rays will generally increase numerical aperture.

It is straightforward to show that, for a light source internal to the fiber core or one in contact with the fiber endface, the alternative expression for the far-field angular transmission is

$$T(\theta) \simeq \frac{1}{n_{co}} \frac{d\theta_{in}}{d\theta} I(\theta_{in}) \left[\frac{F_{TE}(\theta) + F_{TM}(\theta)}{2} \right] \alpha(\theta), \quad (6)$$

where it can be shown that $(d\theta_{in}/d\theta)I(\theta_{in})/n_{co} = I(\theta)/n_{co}^2$ for a Lambertian source.

By evaluating Eq. (4) at numerous sample angles (or equivalently, at sample n_{eff}^r in the range $1 \leq n_{eff}^r \leq n_{co}$), a typical far-field transmission profile as in Fig. 2 is obtained. These curves are usually quite smooth when using a sufficient number of samples, which allows the 5% transmission angle to be easily determined. The NA is then found using Eqs. (1) and (2).

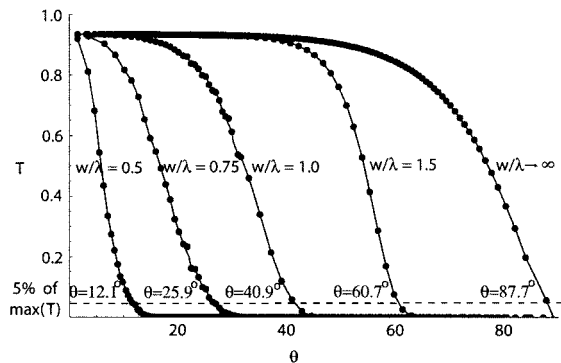


Fig. 2. Typical far-field transmission calculation for a core surrounded by a continuous air ring. $L = 10$ m.

3. Implementation

An adjustable boundary condition method was recently developed¹⁹ in order to accurately and efficiently model confinement loss in microstructured optical fibers. The unique treatment of boundary conditions in this method correctly determines the outward radiating fields of leaky modes without difficult (sometimes manual) searches in the complex n_{eff} plane. This high degree of automation, robustness, and versatility was crucial to the sampling of over 80,000 modes for this paper. While it can be implemented with many numerical mode solvers, the present calculations were conducted using a slight variation on the numerical scheme suggested by Issa *et al.*¹⁹ A radial finite-difference scheme has replaced the basis function expansion, while the azimuthal Fourier expansion is retained. This alternative was adopted after it was found to vastly improve computation speed. The typical resolution of a calculation involves 4000 radial nodes and $10 \times N$ azimuthal Fourier components, where N is the number of bridges and symmetry of the waveguide. The waveguide symmetry is fully exploited to improve computational speed by including only Fourier components that are multiples of N .

Thus over 1600 near-meridional modes were found in the interval $1.0 \leq n_{\text{eff}}^r \leq 1.45$. They were equally sampled from TE_{0n} , TM_{0n} , HE/EH_{1n} , HE/EH_{2n} , and HE/EH_{3n} -like mode classes, with the latter three being doubly degenerate. Additional near-skew mode classes have been shown to negligibly influence the proceeding results. Fixed fiber parameters were core diameter $D_0 = 150 \mu\text{m}$, $n_{\text{co}} = 1.45$, and $\lambda = 1.0 \mu\text{m}$. An advantage of this method is that, from the modal solutions of a given fiber geometry, the length dependence of numerical aperture can be found without further computation. It is emphasized that the number of meridional modes is a small fraction of the total modes. Here $I(\theta) \equiv 1$ is assumed for an isotropic or rotated external source. While it may overestimate the transmission at large angle in some practical situations, the choice is clearly dependent on the system under consideration. However, its influence on the calculated NA has been tracked and found to be not substantial. Therefore this intensity

distribution was adopted to emphasize the influence of other physical factors in the far-field transmission. The major source of inaccuracy in the far-field transmissions, such as Figs. 2 and 3, is in fact the size of the interval $\Delta n_{\text{eff}}^r(\theta)$ used and the discrete number of modes sampled within. The latter consideration is due to the strong polarization dependence of confinement loss. This error typically translates to less than $\pm 2\%$ in the calculated NA.

4. Dependence of NA

When considering microstructured fibers with complex geometries, particularly that shown in Fig. 1(c), it is prudent to first consider the variables on which NA depends. In comparison to the wavelength dependence of the refractive index in the host material, the refractive index contrast with air is very large. This permits a highly profitable simplification owing to wavelength-scale equivalence.²⁰ Without further assumptions, a functional form for a mode effective index is $n_{\text{eff}}(D/\lambda, w/\lambda, \delta/\lambda, N)$, where D is the core diameter, w is the radial width of the hole, δ is the bridge thickness, and N is the number of bridges. Highly multimode fibers generally lie in the extreme of $D/\lambda \gg 1$, where the NA is intuitively weakly dependent on this variable. This was checked and allows this variable to be dropped. However, the appearance of L/λ in Eq. (5) presents an additional variable, which can be equally represented by the more traditional term L/D . It is proportional to the total number of reflections experienced by a meridional ray. Therefore the functional form of numerical aperture becomes simply $\text{NA}(L/D, w/\lambda, \delta/\lambda, N)$. This smaller parameter space is now explored in two

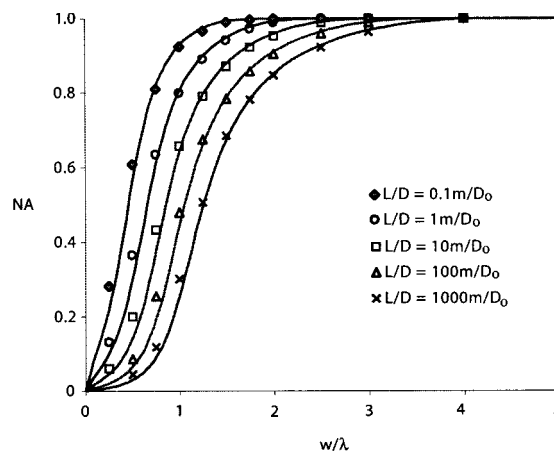


Fig. 3. Example transmission for bridged air-clad fiber. $\delta/\lambda = 0.2$, $N = 75$, $w/\lambda = 8$, and $L/D = 10 \text{ m}/D_0$. (a) Total loss, $-10 \log[T(\theta)]$, as a function of n_{eff} for three mode classes, n_b is the effective index of the fundamental bridge mode, calculated for the equivalent slab waveguide of thickness 0.2. It is a TE mode with respect to the orientation of the slab. n_b^* is the effective index of the second bridge mode, which is a TM mode with respect to the orientation of the slab. (b) Typical transmission curve. Partial transmission after the first sharp drop is due to low-loss TE-like modes and is neglected when measuring the 5% level.

different regimes of operation, which give insight into the design of high NA fibers.

5. Upper Bound on NA

First, the idealized case of a cylindrically symmetric core surrounded by a continuous air ring ($\delta \rightarrow 0, N = 0$) of radial extent, w , is considered. Here optical tunneling (frustrated total internal reflection) is the only loss mechanism, so the purpose of this investigation is twofold. Not only is it instructive of the workings and accuracy of the method in comparison to an alternative, but it also provides an upper bound on the NA achievable in any air-clad fiber whose microstructured cladding is contained within an annulus of width w .

Typical transmission distributions of the leaky-mode method are shown in Fig. 2. As $w/\lambda \rightarrow \infty$, the shape of the transmission curve is dominated by the Fresnel reflections entering and leaving the fiber. For $w/\lambda \leq 2$, confinement loss dominates the shape of the far-field transmission, and the curves slope gently.

A reference chart for the NA in such fibers is given in Fig. 4. Solutions of the local-plane-wave approach are compared with the leaky-mode method. The angular dependence of the plane-wave reflection coefficients in the former method can be found in standard textbooks.²¹ It shows good agreement

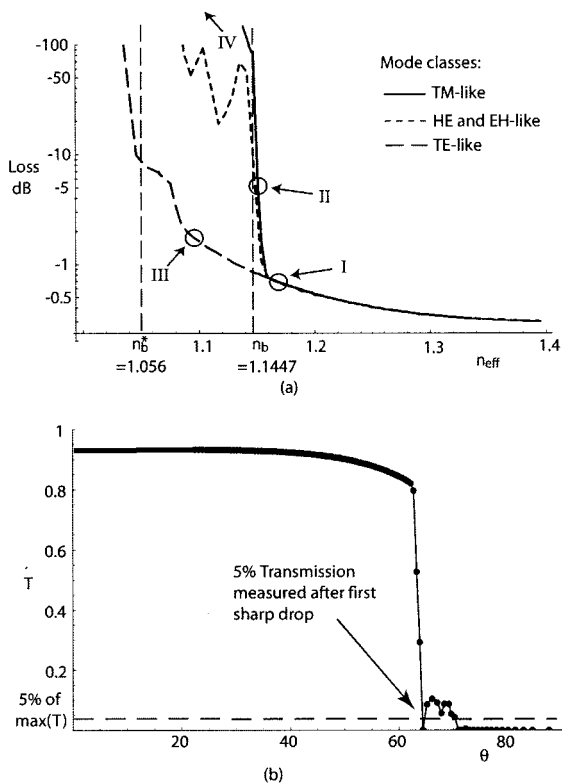


Fig. 4. Numerical aperture of a circular core with continuous air ring of radial width w . Results are obtained by a leaky-mode analysis (points) and the local-plane-wave approach (solid curves). Both show strong length dependence.

mostly for large numerical apertures, where the fiber is highly multimode. An important attribute of the NA in these fibers is the strong length dependence, particularly when $w/\lambda \approx 1$. The upper bounds on NA that it provides are valuable for choosing the radial width of air-clad designs. It suggests that, when $w/\lambda > 4$, the role of optical tunneling in influencing the NA can be neglected for all practical lengths.

6. High NA Air-Clad Fiber: Dependence on Bridge Thickness, Number of Bridges, and Fiber Length

The fiber with bridged cladding is considered here. In order to separate the leakage mechanisms of loss via the bridges from that of optical tunneling, the extreme situation of $w/\lambda \gg 1$ is assumed. Referring to Fig. 4, a choice of $w/\lambda = 8$ is more than adequate for this purpose.

The important loss characteristics for different mode classes in these fibers are shown in the example of Fig. 3(a). It shows two well-defined knees in confinement loss, which are not present in the case of a continuous air ring. The TM-like mode class, as well as the HE and EH-like mode classes, display a knee that coincides with the effective index of the fundamental mode n_b of a slab waveguide of thickness equivalent to the bridges. The slab waveguide representing a bridge is assumed to be oriented radially outward to the fiber. In that sense, the fundamental mode is TE with respect to this orientation. Similarly, the loss curve for the TE-like mode class shows a knee that coincides with the effective index of the second mode of the slab waveguide n_b^* , which is TM with respect to slab orientation. The explanation for this behavior is revealed by considering the local polarizations at the entrance of the bridge; TM-like core modes couple preferentially to TE bridge modes because polarizations are parallel, similar to TE-like core modes and TM bridge modes. Evidently, cross coupling between orthogonal polarizations is greatly suppressed. HE and EH-like core modes, on the other hand, are hybrid and couple efficiently into both bridge modes, yet their loss curve closely follows that of the TM-like core modes.

The direction of power propagation in bridge modes can, in general, have radial and longitudinal components. In the limit of $w/\lambda \rightarrow \infty$, a continuum of these modes exist with effective indices (proportional to the longitudinal component of the wave vector) in the range between 1 and n_b . The effective index n_b is therefore an upper bound for all such localized bridge modes that have a radial component to power propagation. These are expected to rapidly channel power out of core modes with $n_{eff}^r < n_b$ and prevent significant transmission beyond the critical angle dictated by this inequality.

A typical far-field transmission profile is shown in Fig. 3(b). Indicated on the curve is the 5% of maximum transmission point, which is taken after the first sharp drop. Partial transmission after this point is solely due to modes of the TE-like class that continue to possess low confinement loss at angles just beyond

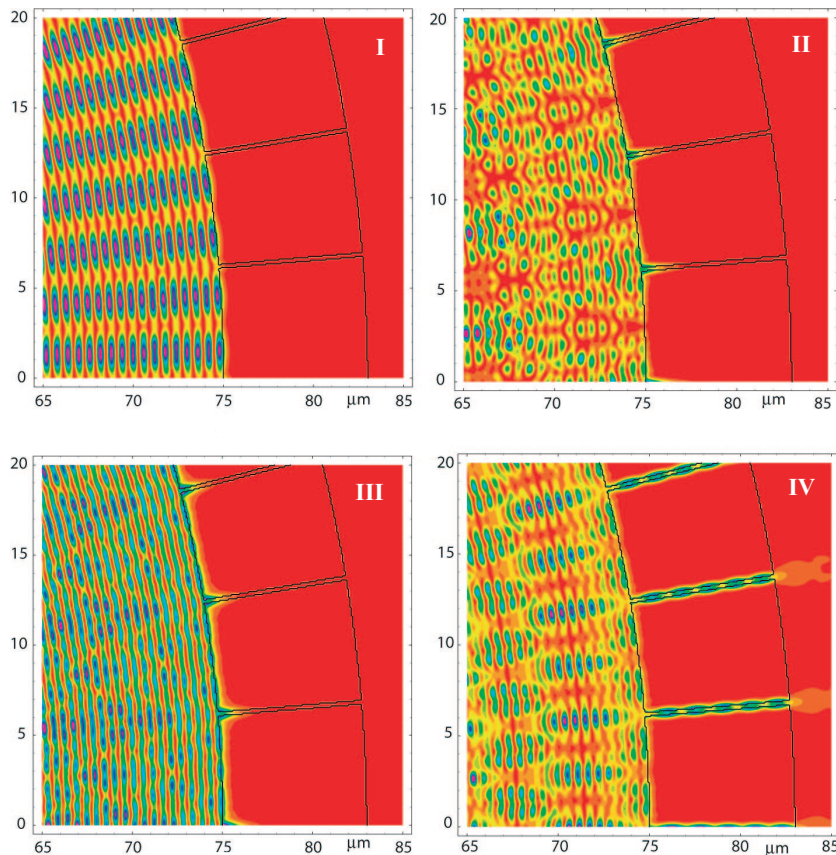


Fig. 5. Example intensity plots of sample core modes in regions I ($n_{\text{eff}}^r \approx 1.175 > n_b$, TM-like mode), II ($n_{\text{eff}}^r \approx 1.1412 = n_b$, TM-like mode), III ($n_{\text{eff}}^r \approx 1.1 < n_b$, TE-like mode) and IV ($n_{\text{eff}}^r \approx 1.1 < n_b$, TM-like mode).

this transition. However, since the TE-like modes constitute a small fraction of the total modes, they make a negligible contribution to transmission as more mode classes are included. The choice of 5% transmission at the first sharp drop is therefore justified.

To investigate the evolution of the leaky-mode solutions in the neighborhood of this transition, four locations are chosen, and the mode intensities are plotted in Fig. 5. The plots confirm that the transitions in loss seen in Fig. 3(a) signal the efficient launching of power into local bridge modes. Strong coupling between TM-like core modes and the TE bridge mode is seen, while TE-like core modes remain well confined until a TM bridge mode is supported. Often the difference in loss between TE and TM-like core modes can be orders of magnitude for nearly equal n_{eff}^r . This effect disappears for thicker bridges that support many closely spaced TE and TM modes.

Finally, a chart showing the dependence of numerical aperture on bridge thickness and fiber length is given in Fig. 6. It shows that NA is strongly dependent on bridge thickness and that $\delta/\lambda \ll 1$ is required for NAs close to 1. On the other hand, the length dependence is very weak for all practical lengths and only becomes significant for small NA. The number of bridges also proved to be a weak dependence. For $N = 50, 75,$ and 100 , the calculated NA differed by less than a few percent for all lengths. Both these

findings are consistent with the qualitative observation of a very sharp increase in confinement loss at a particular angle. Also plotted is the heuristic expression $\bar{\text{NA}} = (n_{\text{co}}^2 - n_b^2)^{1/2}$, obtained from the

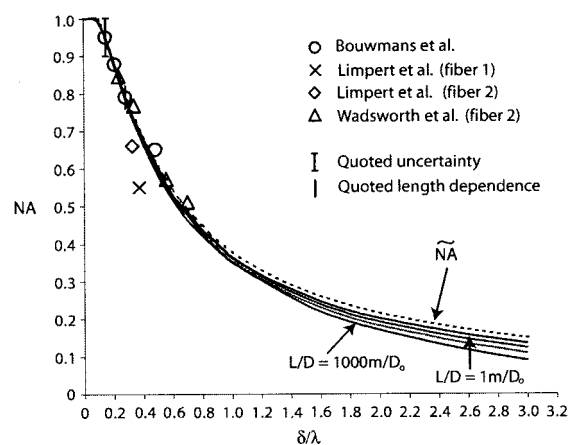


Fig. 6. Full calculation of NA and comparison with measured values. The vertical bar through experimental data indicates the range of measured values for different fiber lengths (when quoted). Shown are $L/D = 1 \text{ m}/D_0, 10 \text{ m}/D_0, 100 \text{ m}/D_0,$ and $1000 \text{ m}/D_0$ for $w/\lambda = 8$. Calculations for $N = 50, 75,$ and 100 are nearly indistinguishable. The $\bar{\text{NA}} = (n_{\text{co}}^2 - n_b^2)^{1/2}$ curve is obtained from the fundamental bridge mode.

fundamental bridge mode. As expected, it provides a close upper bound on the calculated NA.

Most importantly, the published results of NA measurements on similar fibers are compared. The fiber presented by Bouwmans *et al.*⁷ is the closest in geometry and shows excellent agreement with calculations. The fibers of Wadsworth *et al.*^{6,8} and Limpert *et al.*¹⁰ (fibers 1 and 2) differ slightly in that they also contain microstructure in the core and have a hexagonally shaped cladding. Nevertheless, the agreement is good to fair, which suggests the results may be applicable to a wider class of fiber geometries.

A measurable length dependence of NA has been reported. When values are given, the quoted range of measured NA is indicated in Fig. 6 with a vertical bar. However, the magnitude of NA variation with length exceeds numerical predictions. This is likely due to the inevitable launching of skew rays, which will generally increase the measured NA for short lengths of fiber but quickly degrade to the meridional NA. The rapid loss of skew rays is due to the relatively larger number of reflections experienced along their helical path. Alternatively, coupling between modes as a result of fiber nonuniformities and surface scattering is another contributing factor. The influence of such effects is beyond the scope of this paper and has been so far neglected. Measurement error is another important factor in determining the significance of such discrepancies. Sources of error may include fiber nonuniformity, improper launching, and inaccuracy in the measurement of bridge thickness or NA. These errors have so far not been discussed or quantified in the literature.

7. Conclusions

A new method employing leaky modes has been used to determine the numerical aperture in highly multimode air-clad microstructured fibers. Accurate results have been obtained that show the numerical aperture to be weakly dependent on fiber length and the number of bridges. However, the dependence on bridge thickness is strong and shows that an exceptionally high NA can be achieved only for bridge thicknesses much smaller than the wavelength. The physical basis of these key results is understood in terms of the conditions for efficient excitation of bridge local modes that radially propagate power into the outer jacket. A comparison is made with published measurements of NA on similar fibers, which show excellent and robust agreement.

Valuable discussions with W. E. Padden, K. F. Klein, M. A. van Eijkelenborg, A. Argyros, and I. M. Bassett are thankfully acknowledged, as well as financial support from Redfern Photonics and the Australian Research Council.

References

1. C. P. Achenbach and J. H. Cobb, "Computational studies of light acceptance and propagation in straight and curved multimode active fibers," *J. Opt. A* **5**, 239–249 (2003).
2. E. Mediavilla, S. Arribas, and F. Watson, *Fiber Optics in Astronomy* (Astronomical Society of the Pacific, San Francisco, Calif., 1998), Vol. 3.
3. J. K. Sahu, C. C. Renaud, K. Furusawa, R. Selvas, J. A. Alvarez-Chavez, D. J. Richardson, and J. Nilsson, "Jacketed air-clad cladding pumped ytterbium-doped fiber laser with wide tuning range," *Electron. Lett.* **37**, 1116–1117 (2001).
4. N. A. Mortensen, M. Stach, J. Broeng, A. Petersson, H. R. Simonsen, and R. Michalzik, "Multi-mode photonic crystal fibers for VCSEL based data transmission," *Opt. Express* **11**, 1953–1959 (2003).
5. D. Feuermann, J. M. Gordon, and M. Huleihil, "Light leakage in optical fibers: experimental results, modeling and the consequences for solar collectors," *Solar Energy* **72**, 195–204 (2002).
6. W. J. Wadsworth, R. M. Percival, G. Bouwmans, J. C. Knight, and P. St. J. Russell, "High power air-clad photonic crystal fiber laser," *Opt. Express* **11**, 48–53 (2003).
7. G. Bouwmans, R. M. Percival, W. J. Wadsworth, J. C. Knight, and P. St. J. Russell, "High-power Er:Yb fiber laser with very high numerical aperture pump-cladding waveguide," *Appl. Phys. Lett.* **83**, 817–818 (2003).
8. W. J. Wadsworth, R. M. Percival, G. Bouwmans, J. C. Knight, T. A. Birks, T. D. Hedley, and P. St. J. Russell, "Very high numerical aperture fibers," *IEEE Photon. Technol. Lett.* **16**, 843–845 (2004).
9. K. Furusawa, A. Malinowski, J. H. V. Price, T. M. Monro, J. K. Sahu, J. Nilsson, and D. J. Richardson, "Cladding pumped ytterbium-doped fiber laser with holey inner and outer cladding," *Opt. Express* **9**, 714–720 (2001).
10. J. Limpert, T. Schreiber, A. Liem, S. Nolte, H. Zellmer, T. Peschel, V. Guyenot, and A. Tünnermann, "Thermo-optical properties of air-clad photonic crystal fiber lasers in high power operation," *Opt. Express* **11**, 2982–2990 (2003).
11. E. A. J. Marcatili, "Air clad optical fiber waveguide," U.S. patent 3,712,705 (23 January 1973).
12. R. J. Potter, "Transmission properties of optical fibers," *J. Opt. Soc. Am.* **51**, 1079–1089 (1961).
13. N. A. Mortensen, J. R. Folkenberg, P. M. W. Skovgaard, and J. Broeng, "Numerical aperture of single-mode photonic crystal fibers," *IEEE Photon. Technol. Lett.* **14**, 1094–1096 (2002).
14. A. W. Snyder and J. D. Love, *Optical Waveguide Theory* (Chapman & Hall, London, 1983), Chap. 24.
15. R. Sammut and A. W. Snyder, "Leaky modes on a dielectric waveguide: orthogonality and excitation," *Appl. Opt.* **15**, 1040–1044 (1976).
16. A. W. Snyder and J. D. Love, *Optical Waveguide Theory* (Chapman & Hall, London, 1983), Chaps. 4 and 20.
17. J. A. Buck, "Fundamentals of optical fibers," (Wiley, New York, 1995), pp. 49–51.
18. R. L. Gallawa, "On the definition of fiber numerical aperture," *Electro-Opt. Syst. Des.* **14**, 46–54 (1982).
19. N. A. Issa and L. Poladian, "Vector wave expansion method for leaky modes of microstructured optical fibers," *J. Lightwave Technol.* **21**, 1005–1012 (2003).
20. K. Sakoda, *Optical Properties of Photonic Crystals* (Springer, Berlin, 2001), pp. 21–23.
21. E. Hecht, *Optics*, 3rd ed. (Addison-Wesley, Reading, Mass., 1998), pp. 419–420.